IOP PUBLISHING PHYSICS IN MEDICINE AND BIOLOGY

Phys. Med. Biol. **53** (2008) 4063–4080 doi:10.1088/0031-9155/53/15/004

Quantitative sonoelastography for the *in vivo* assessment of skeletal muscle viscoelasticity

Kenneth Hoyt[1,2], Timothy Kneezel[3], Benjamin Castaneda[2] and Kevin J Parker[2]

[1] Department of Radiology, University of Alabama at Birmingham, Birmingham, AL 35294, USA
[2] Department of Electrical and Computer Engineering, University of Rochester, Rochester, NY 14627, USA
[3] Department of Biomedical Engineering, University of Rochester, Rochester, NY 14627, USA

Received 14 December 2007, in final form 5 June 2008
Published 8 July 2008
Online at stacks.iop.org/PMB/53/4063

Abstract

A novel quantitative sonoelastography technique for assessing the viscoelastic properties of skeletal muscle tissue was developed. Slowly propagating shear wave interference patterns (termed crawling waves) were generated using a two-source configuration vibrating normal to the surface. Theoretical models predict crawling wave displacement fields, which were validated through phantom studies. In experiments, a viscoelastic model was fit to dispersive shear wave speed sonoelastographic data using nonlinear least-squares techniques to determine frequency-independent shear modulus and viscosity estimates. Shear modulus estimates derived using the viscoelastic model were in agreement with that obtained by mechanical testing on phantom samples. Preliminary sonoelastographic data acquired in healthy human skeletal muscles confirm that high-quality quantitative elasticity data can be acquired *in vivo*. Studies on relaxed muscle indicate discernible differences in both shear modulus and viscosity estimates between different skeletal muscle groups. Investigations into the dynamic viscoelastic properties of (healthy) human skeletal muscles revealed that voluntarily contracted muscles exhibit considerable increases in both shear modulus and viscosity estimates as compared to the relaxed state. Overall, preliminary results are encouraging and quantitative sonoelastography may prove clinically feasible for *in vivo* characterization of the dynamic viscoelastic properties of human skeletal muscle.

(Some figures in this article are in colour only in the electronic version)

1. Introduction

Palpation is a clinical procedure that dates back to antiquity. This routine physical examination allows clinicians to subjectively evaluate the tactile response of soft tissues whereby suspicious

tissues or masses are typically identified for further evaluation or monitoring. The utility of palpation as a diagnostic tool is founded on the elastic properties of soft tissues, namely local shear modulus distributions. Since the shear modulus of various soft tissues spans several orders of magnitude (Sarvazyan *et al* 1998), a fundamental elastic contrast manifests between normal human tissue types. Moreover, many pathological conditions are associated with a marked change in the tissue elastic properties (Krouskop *et al* 1998, Phipps *et al* 2005, Zhang *et al* 2008), which may be exploited for detection purposes. Notwithstanding, the efficacy of palpation-based examinations is typically limited to detection and qualitative assessment of superficial tissues or structures.

Throughout the last two decades numerous imaging-based methods have been introduced for estimating and visualizing the elastic properties of soft tissue (Gao *et al* 1996, Ophir *et al* 1999, Greenleaf *et al* 2003). The generalized premise behind these elasticity imaging techniques is to apply a mechanical stimulus (either static or dynamic stress distribution) to the target tissue and, subsequently, image the deformation response using either ultrasound or nuclear magnetic resonance technology. In particular, sonoelastography is an elasticity imaging method that utilizes Doppler ultrasonic techniques to estimate tissue motion (in the form of propagating shear waves) induced using low-amplitude and low-frequency external vibrational sources (Lerner *et al* 1988). Using a modified pulsed Doppler ultrasound system, local qualitative estimates of tissue elasticity can be imaged (termed a sonoelastogram) in real-time to reflect relative changes in tissue stiffness. In practice, when a region of tissue contains a stiff lesion or mass, a local decrease in the shear wave displacement amplitude results (Parker *et al* 1998). More recently, crawling wave sonoelastography was developed and introduced (Wu *et al* 2004). With this modality, slowly moving shear wave interference patterns (termed crawling waves) are generated using a pair of mechanical sources and imaged using sonoelastography. The main advantage to this sonoelastographic development is that crawling wave spatial properties (namely wavelength) reflect local tissue elastic properties (Wu *et al* 2006). Integration of crawling wave principles and a computationally efficient phase-based shear wave speed estimator allowed realization of quantitative sonoelastographic imaging (Hoyt *et al* 2007a, 2008).

Demonstration of *in vivo* muscle tissue characterization using elasticity imaging-based techniques has been reported by several research groups (Levinson *et al* 1995, Kruse *et al* 2000, Dresner *et al* 2001, Basford *et al* 2002, Sack *et al* 2002, Gennisson *et al* 2003, Heers *et al* 2003, Jenkyn *et al* 2003, Bensamoun *et al* 2006, 2007, Hoyt *et al* 2007b). However, knowledge regarding the *in vivo* viscoelastic properties of human skeletal muscles is still very limited, which may be attributed to a lack of repeatable techniques permitting quantitative assessment of muscle function noninvasively. Potential applications for *in vivo* skeletal muscle assessment may include sports training in relation to strength and endurance exercise regimens, physical therapy planning and treatment efficacy, and progression of degenerative diseases such as muscular dystrophy. Therefore, the motivation for this research project was to develop and evaluate a novel quantitative sonoelastographic technique for *in vivo* characterization of skeletal muscle tissue.

2. Theory

2.1. Principles of sonoelastography

In conventional sonoelastographic imaging, low-frequency mechanical vibrations are used to noninvasively excite shear wave propagation in tissue. Given the tissue stress response from shear wave motion, qualitative sonoelastographic images (termed sonoelastograms)

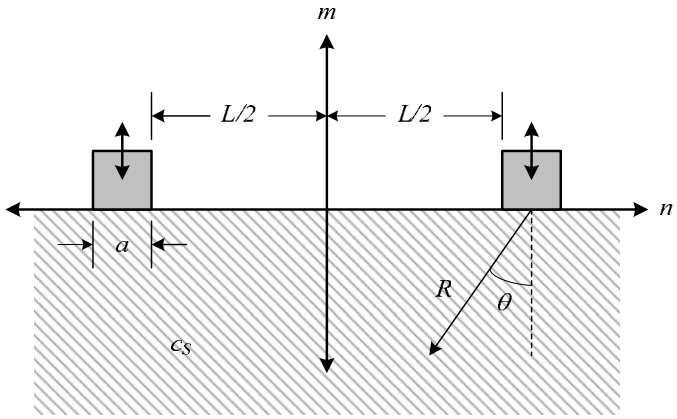

Figure 1. Illustration of coordinate system and variables used to derive shear displacement fields for a two-source mechanical system vibrating normal (double arrows) to a free boundary.

are generated using ultrasonic Doppler techniques. As reported previously, the vibrational amplitude of tissue scatterers in oscillatory motion alters the power spectrum of an insonating ultrasound beam in a predictable manner (Huang *et al* 1990). Specifically, a linear relationship exists between the vibrational amplitude u and standard deviation σ of the backscattered power spectrum as follows:

$$u = \frac{1}{4\sqrt{2}\pi^2}\frac{c_L\sigma}{f_L f_S}, \tag{1}$$

where c_L, f_L and f_S denote the longitudinal wave propagation speed in the medium being investigated, the frequency of the longitudinal wave and the frequency of the shear wave, respectively. Equation (1) represents the governing principle behind sonoelastographic imaging whereby the amplitude of a vibrating target is determined indirectly using a spectral variance estimator (Kasai *et al* 1985):

$$\sigma^2 = \frac{2}{T_{\mathrm{PRF}}^2}\left(1 - \frac{|\hat{R}(T_{\mathrm{PRF}})|}{\hat{R}(0)}\right), \tag{2}$$

where T_{PRF} is the time interval at which ultrasonic pulses are emitted and $\hat{R}$ is the autocorrelation function of the backscattered signal for a given packet size (typically ranges from 8 to 16 samples as defined by the imaging system). Using a larger packet size improves the statistical properties of the autocorrelation-based estimator but lowers the imaging frame rate for a given region-of-interest (ROI). In sonoelastographic imaging it is the spectral variance parameter that is visualized, which is proportional to the magnitude squared of the shear displacement field (Taylor *et al* 2000). By utilizing equation (2), a modified pulsed Doppler ultrasound system allows real-time sonoelastographic imaging.

2.2. Shear wave excitation using normal vibration

In order to represent the shear displacement fields for a two-source configuration we take advantage of Miller and Pursey's (1954) early work on mechanical radiators. Assuming a farfield approximation, the shear displacement fields are calculated as a function of the coordinates, dimensions of the radiator and the elastic properties of the medium (see figure 1).

Consider a long thin strip of width a placed in contact with a semi-infinite, homogeneous and isotropic elastic solid and vibrating normal to the surface of the medium with unity boundary stress and frequency f_S. Neglecting contributions from propagating longitudinal waves, instantaneous shear displacement fields for the m and n components are approximated as follows (Miller and Pursey 1954):

$$u_m(m,n,t) = \frac{a\exp\left(\frac{i\pi}{4}\right)\cos\theta}{k_L c_S}\sqrt{\frac{2}{\pi k_L R}}\frac{2k^{5/2}\sin^2\theta\sqrt{k^2\sin^2\theta-1}}{F(k\sin\theta)}\exp(i[2\pi f_S t - k_S R]), \tag{3}$$

and

$$u_n(m,n,t) = -\frac{a\exp\left(\frac{i\pi}{4}\right)\cos\theta}{k_L c_S}\sqrt{\frac{2}{\pi k_L R}}\frac{k^{5/2}\sin 2\theta\sqrt{k^2\sin^2\theta-1}}{F(k\sin\theta)}\exp(i[2\pi f_S t - k_S R]), \tag{4}$$

where

$$F(\xi) = \left(2\xi^2 - k_S^2\right)^2 - 4\xi^2\sqrt{(\xi^2-1)\left(\xi^2-k_S^2\right)},$$

$i = \sqrt{-1}$, c_S is the shear wave propagation speed in the medium, k_L and k_S are the longitudinal and shear wave numbers, respectively, $k = k_S/k_L$, $R = \sqrt{m^2+n^2}$, $\theta = \tan^{-1}(n/m)$ and t denotes time. Throughout this paper, coordinates defined by m and n will consistently refer to the axial and lateral image dimensions, respectively.

Due to practical considerations, we restrict our attention to equation (3) to introduce the displacement fields for a two-source configuration. With this approach, particle vibration is normal to the free boundary or tissue surface and allows visualization using sonoelastographic techniques. To represent the displacement fields, we define a source separation distance L (see figure 1) and utilize the principle of superposition to describe the instantaneous shear wave interference patterns as

$$u_m(m,n,t) = u_m\left(m+\frac{L}{2},n,t\right) + u_m\left(\frac{L}{2}-m,n,t\right). \tag{5}$$

As indicated in section 2.1, the magnitude squared of the shear displacement field is estimated using sonoelastographic techniques, so we describe the instantaneous interfering shear displacement fields alternatively as follows:

$$\begin{aligned}|u_m(m,n,t)|^2 = &\left[u_m\left(m+\frac{L}{2},n,t\right) + u_m\left(\frac{L}{2}-m,n,t\right)\right]\\ &\times\left[u_m^*\left(m+\frac{L}{2},n,t\right) + u_m^*\left(\frac{L}{2}-m,n,t\right)\right],\end{aligned} \tag{6}$$

where u^* is the complex conjugate of u. As noted in Hoyt *et al* (2007a) for interfering plane waves, the magnitude squared operation allows recovery of a harmonic signal from the estimated displacement amplitudes while producing a doubling of the shear wave interference pattern spatial frequency.

2.3. Crawling wave phenomena

It has been shown that shear wave interference patterns can be generated by two coherent monochromatic vibration sources and imaged using sonoelastography (Wu *et al* 2004). Moreover, if the two sources vibrate at slightly offset frequencies, e.g. f_S and $f_S + \Delta f_S$,

then the interference patterns slowly propagate at an apparent speed equal to $c_S \cdot \Delta f_S/2f_S$. These moving shear wave interference patterns have been termed crawling waves. In practice, the frequency difference Δf_S is chosen to be less than $f_S/500$ since using a higher frequency offset may compromise imaging results due to presence of a beat frequency. Owing to the properties of these interfering shear waves, the local spacing between the pattern bands equals half of the shear wavelength λ. Therefore, analysis of the local shear wave interference patterns (or crawling wave image frames) allows estimation of the governing shear wave propagation speed or modulus μ_1 distribution as follows:

$$c_S = \sqrt{\frac{\mu_1}{\rho}} = 2f_S\lambda. \tag{7}$$

where ρ denotes the tissue mass density. It is important to note that equation (7) assumes that the biomechanical properties of tissue are isotropic and linear elastic (i.e., nonviscous), characterized by knowledge of either the shear wave speed or modulus parameter. However, most biological tissues exhibit viscoelastic properties that introduce a frequency dependence for dynamic mechanical property measurements. Additionally, tissues such as skeletal muscle are anisotropic due to fascicle ordering and measurements are further governed by fiber orientation. Therefore, tissue characterization predicated solely on the analysis of crawling wave images using equation (7) may be insufficient and a more accurate approach may be warranted (see section 2.5).

2.4. Quantitative sonoelastography

Analysis of crawling wave spatial patterns allows estimation of the local elastic properties for a material or tissue being investigated. Given shear wave interference displacement fields, it was shown in Hoyt *et al* (2008) that the shear wave speed distribution in 2D space can be estimated by evaluating the phase of the 2D autocorrelation function $\widehat{\gamma}(m', n')$ of the analytic signal $\hat{u}(m, n)$,

$$\widehat{\gamma}(m', n') = \sum_{m=0}^{M-m'-1} \sum_{n=0}^{N-n'-1} \hat{u}^*(m, n)\hat{u}(m + m', n + n'), \tag{8}$$

at lags $(m' = 1, n' = 0)$ and $(m' = 0, n' = 1)$. Note that the analytic signal used in equation (8) is computed using a 1D fast Fourier transform method introduced by Marple (1999) applied along the shear wave propagation axis (assumed to be n) for each depth location of the acquired crawling wave image (Hoyt *et al* 2007a). Equation (8) assumes that the observation window consists of M axial samples $(m = 0, 1, \ldots, M - 1)$ and N lateral samples $(n = 0, 1, \ldots, N - 1)$. The mean shear wave speed components $\langle c_S \rangle_m$ and $\langle c_S \rangle_n$ are estimated independently and relative to the m- and n-axes, respectively, and are given by the following expressions:

$$\langle c_S \rangle_m = \left| \frac{2\pi(2f_S + \Delta f_S)T_m}{\tan^{-1}\left\{\frac{\mathrm{Im}[\hat{\gamma}(1,0)]}{\mathrm{Re}[\hat{\gamma}(1,0)]}\right\}} \right|, \tag{9}$$

and

$$\langle c_S \rangle_n = \left| \frac{2\pi(2f_S + \Delta f_S)T_n}{\tan^{-1}\left\{\frac{\mathrm{Im}[\hat{\gamma}(0,1)]}{\mathrm{Re}[\hat{\gamma}(0,1)]}\right\}} \right|. \tag{10}$$

where T_m and T_n are the spatial sampling rates in the m and n dimensions, respectively. Using equations (9) and (10), the 2D mean shear wave speed estimate $\langle c_S \rangle_{2D}$ can be described by the

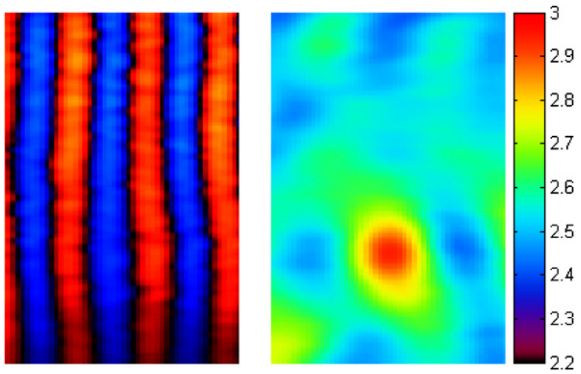

Figure 2. (a) Crawling wave sonoelastogram depicting shear wave interference patterns in a tissue-mimicking gelatin phantom with an embedded 5 mm diameter spherical inclusion of stiffer gelatin. Shear waves were excited using a vibration frequency of 200 Hz and local image properties (namely spatial wavelength) reflect the material's elastic properties. (b) Quantitative sonoelastogram (averaged over one wavelength of crawling wave motion) depicting the shear velocity distribution (unit of $\mathrm{m\,s^{-1}}$) within the heterogeneous phantom material. The estimated shear wave speed of the stiff inclusion is approximately 1.5 times higher than the surrounding material.

following expression (Hoyt *et al* 2008),

$$\langle c_S \rangle_{2D} = \frac{\langle c_S \rangle_m}{\sqrt{\left(\frac{\langle c_S \rangle_m}{\langle c_S \rangle_n}\right)^2 + 1}}, \tag{11}$$

indicating that the 2D local shear wave speed can be estimated from the spatial shear wave interference patterns given knowledge of the source vibration frequencies and spatial sampling rate. In the derivation of equation (11) we assume that within the region defined by our kernel size that the tissue property is approximately homogeneous and that the local shear wave interference patterns can be approximated as plane waves (regardless of angular orientation relative to the transducer axis). Since equation (11) produces a local shear wave speed estimate, 2D spatial distributions are obtained by one-sample shifting the kernel throughout the shear wave displacement field. Note that for interference patterns (i.e., plane waves) oriented parallel to the imaging axis, $\langle c_S \rangle_n$ approaches infinity and $\langle c_S \rangle_{2D}$ is equal to $\langle c_S \rangle_m$. Although sonoelastography only detects tissue vibration normal to the imaging transducer, shear waves can propagate along complicated paths owing to internal and external boundary conditions, diffraction, etc. Therefore, for angulated plane waves or interference patterns exhibiting distorted wavefronts, $\langle c_S \rangle_n$ is finite valued and estimation of the 2D mean shear wave speed using equation (11) allows for an accurate description of the true underlying shear wave speed distribution (Hoyt *et al* 2008).

A representative set of matched experimental crawling wave and quantitative sonoelastograms from a heterogeneous tissue-mimicking elasticity phantom are illustrated in figure 2. As this image depicts, quantitative sonoelastography has the potential to detect stiff lesions with diameters as small as 5 mm. However, detectibility is ultimately governed by lesion-background modulus contrast, source vibration frequency and estimator kernel size (Hoyt and Parker 2007).

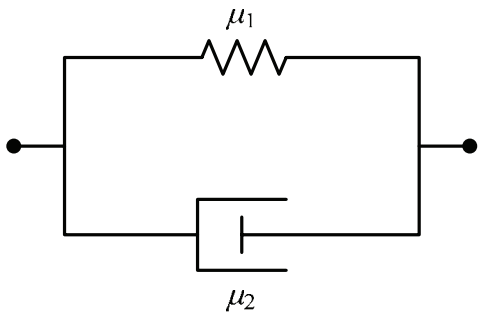

Figure 3. Viscoelastic model for a Voigt body where μ_1 and μ_2 are the coefficients of elasticity and viscosity, respectively.

2.5. Viscoelasticity estimation

Quantitative sonoelastography produces detailed images that reflect tissue shear wave speed distributions. However, biological tissues exhibit shear wave speed dispersion suggesting that a viscoelastic model may be used to quantify the complex stiffness, or more specifically, tissue elasticity and viscosity coefficients. Interested readers are referred to Fung (1993) and Lakes (1998) for a thorough review of the viscoelastic properties of biological tissues. For the purposes of this paper, it was assumed that tissue (or biomaterial) could be modeled as a Voigt body, which consists of a linear elastic spring in parallel with a viscous dashpot (figure 3). For a homogeneous medium, the shear wave speed for the Voigt model is related to the vibration frequency by Oestreicher (1951):

$$c_S = \sqrt{\frac{2\left(\mu_1^2 + f_S^2\mu_2^2\right)}{\rho\left(\mu_1 + \sqrt{\mu_1^2 + f_S^2\mu_2^2}\right)}} \tag{12}$$

where μ_2 denotes the shear viscosity. Note that in the absence of tissue viscosity (i.e., $\mu_2 = 0$), equation (12) simplifies to the expression described by equation (7). The viscoelastic model described by equation (12) has been shown in the literature to be a promising technique for estimating the frequency-independent shear modulus and shear viscosity parameters of various biological tissues including skeletal muscle (Madsen *et al* 1983, Kruse *et al* 2000, Catheline *et al* 2004, Gennisson *et al* 2006, Greenleaf and Chen 2007).

3. Simulations

A sonoelastographic simulation program was implemented using Matlab 7.0 (Mathworks, Inc., Natick, MA, USA) and based on the analysis presented in section 2.2. For all simulation results, the shear wave signal-to-noise ratio (SNR) was established by superimposing Gaussian noise onto the shear wave displacement fields. All default simulation parameters are listed in table 1 unless otherwise stated.

Utilizing the principles of superposition, shear wave displacement fields for a two-source configuration (separation distance L of 11 cm) as described by equation (6) were generated (figure 4). Figure 4(a) indicates that shear wave interference patterns are localized at depth to a region between the surface contacts of the oscillating sources. Although not illustrated, increasing the source separation distance allows penetration and displacement of deeper regions. However, elevated shear wave attenuation effects due to increased propagation distances may compromise crawling wave SNR levels in practice. Regarding figure 4(a),

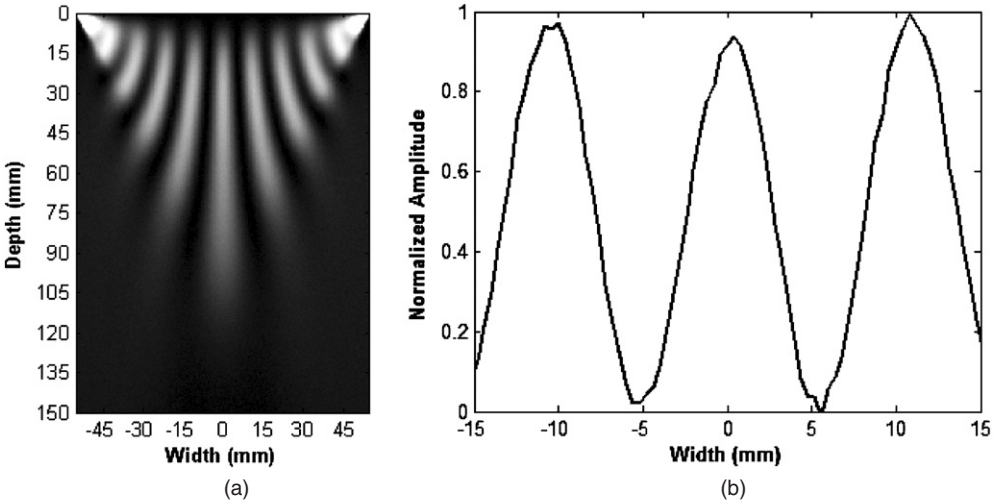

Figure 4. Simulated (a) crawling wave sonoelastogram for a source vibration frequency of 140 Hz and (b) cross-sectional shear wave interference displacement profile extracted at a depth of 15 mm. The true shear wave speed was simulated at 3 m s^{-1}.

Table 1. Default values used for simulation studies.

Parameter	Value
Source separation (L)	11 cm
Source contact diameter (a)	0.8 cm
Mass density (ρ)	1000 kg m^{-3}
Shear wave speed (c_S)	3 m s^{-1}
Vibration frequency (f_S)	140 Hz
Axial spatial sampling interval (T_m)	400 μm
Lateral spatial sampling interval (T_n)	400 μm
Axial kernel dimension (M)	24 samples
Lateral kernel dimension (N)	24 samples
Signal-to-noise ratio (SNR)	40 dB

results indicated that at depths proximal to the upper boundary (e.g. between depths of 5 and 30 mm) a plane wave assumption may be inferred. Pattern spreading and wavelength elongation nullifies this assumption for deeper regions. In order to investigate the validity of the plane wave assumption, a cross-sectional shear wave interference displacement profile (extracted from figure 4(a) at a depth of 15 mm) is plotted in figure 4(b). Since the shear wave speed of the material was 3 m s^{-1} and the spatial wavelength measured from these plots was 10.7 mm, the ratio of these two quantities yields a temporal frequency of 280 Hz. Therefore, the spatial frequency exhibited by shear wave interference patterns excited using a two-source configuration appears to be twice the source vibration frequency (140 Hz for the results presented), where plane wave conditions can be assumed valid. This fundamental frequency relationship supports using the 2D shear wave speed sonoelastographic estimation technique since it was implicit in algorithm development (Hoyt *et al* 2008).

Adopting a field-of-view representative of that employed during ultrasonic imaging of superficial tissues and positioned equidistant from mechanical sources, crawling wave sonoelastograms were simulated for the two-source shear wave excitation configuration

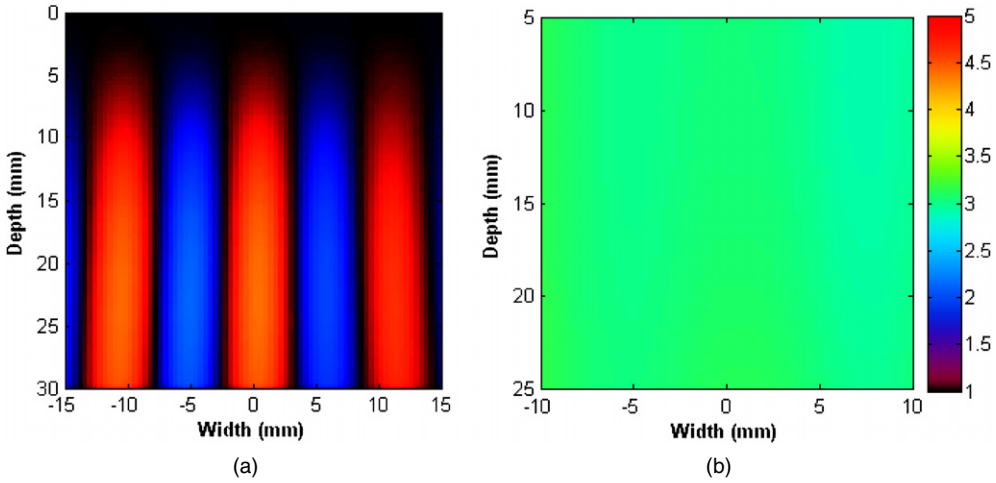

Figure 5. Simulated (a) crawling wave and (b) shear wave speed sonoelastogram for a source vibration frequency of 140 Hz. The true shear wave speed was simulated at 3 m s^{-1}.

(figure 5). Subsequently, the shear wave speed distribution was reconstructed using the 2D quantitative sonoelastography technique described in section 2.4. Despite minimal displacement information in the nearfield of the crawling wave sonoelastograms (simulation assumes farfield conditions) the shear wave speed sonoelastograms exhibit a uniform distribution throughout the image plane. Specifically, the average shear wave speed computed from the simulation-based sonoelastogram in figure 5(b) was found to be 3.07 $\pm$ 0.11 m s^{-1}, which agrees with the true shear wave speed of 3 m s^{-1} (2.3% error).

4. Experiments

For experimental studies, sonoelastographic results were obtained using the setup illustrated in figure 6. A two-channel signal generator (Model AFG320, Tektronix, Beaverton, OR, USA) produced two monochrome low frequency signals that were passed through power amplifiers (Model 2706, Brüel & Kjær, Nærum, Denmark) before being input to the vibration sources (Model 4810, Brüel & Kjær, Nærum, Denmark). The source contacts were square aluminum bars measuring 10 mm in width and 60 mm in length with the long axis oriented orthogonal to the imaging plane. The source separation distance was fixed at 11 cm. Shear wave propagation was excited using an incremented vibration frequency range of 80 to 200 Hz (in 20 Hz increments) with a frequency difference (offset) set at 0.2%. Source amplitudes (nominally less than 200 μm) were adjusted for each vibration frequency and prior to data collection to produce well-formed shear wave interference patterns (i.e., maximal visible SNR) for a given field-of-view. A modified GE Logiq 9 ultrasound system (GE Medical Systems, Milwaukee, WI) was employed for scanning with demodulated colorflow data saved for offline processing. From all acquired data sets, shear wave speed sonoelastograms were computed from the reconstructed sonoelastographic crawling wave images using the 2D autocorrelation-based estimation technique (see section 2.4). A fixed kernel size of 24 by 24 samples (approximately 1.0 cm^2) was utilized in order to minimize estimator noise levels (Hoyt *et al* 2008). Prior to processing, all data sets were downsampled in the axial dimension to closely match the sampling rate in the lateral dimension and to minimize computation time. Note that this downsampling was determined to have minimal effects on sonoelastographic

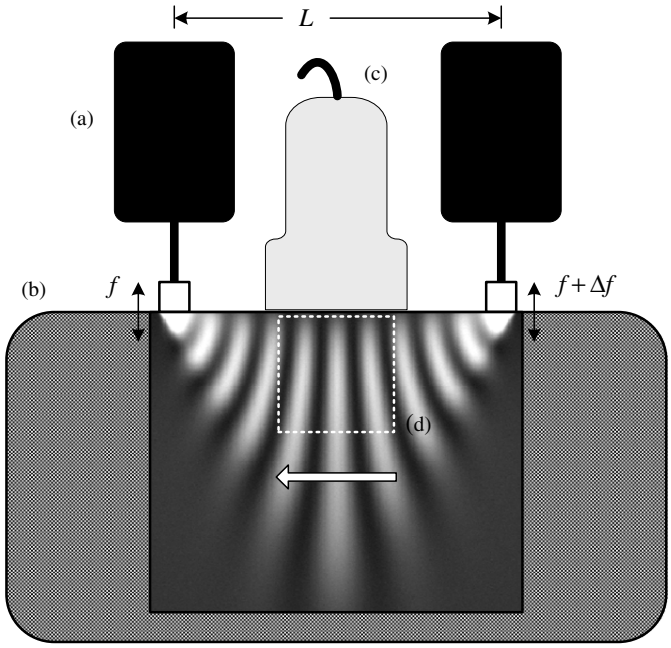

Figure 6. Illustration of the setup used to produce sonoelastographic crawling waves in experiments. Two mechanical sources (a) separated by distance L vibrate at slightly offset frequencies (double arrows) and coupled normal to the free surface of the imaging material (b). Slowly moving shear wave displacement fields are imaged using an ultrasound probe (c) for a given region-of-interest (d) as these crawling wave propagate through the medium (large arrow).

results since the spatial information of interest is predominately in the crawling wave lateral dimension. Statistics were computed from shear wave speed sonoelastogram sequences (equating to one spatial wavelength of crawling wave motion). Lastly, using the dispersive shear wave speed sonoelastographic data (i.e., mean values), frequency-independent shear elasticity and shear viscosity estimates were obtained using the viscoelastic model described by equation (12) and data fitting using the Gauss–Newton method for nonlinear least-squares. Specifically, individual shear wave speeds were obtained for a range of vibration frequencies and this data set leads to a single mathematical expression based on equation (12). The mass density of skeletal muscle tissue was assumed constant at 1100 kg m^{-3}.

4.1. Phantom studies

In the phantom studies, experimental results were obtained using a homogeneous gelatin-based elasticity phantom with the ultrasound transducer rigidly fixed equidistant from the source contacts. Note that the transducer was isolated from the mechanical sources in order to minimize vibration coupling. Mechanical tests using a $1/S$ mechanical device (MTS Systems Co., Eden Prairie, MN, USA) equipped with a 5 Newton load cell were performed on a phantom sample in order to approximate the true elastic properties for comparison to imaging results.

The results in figure 7 depict representative experimental crawling wave and shear wave speed sonoelastograms for a vibration frequency of 140 Hz. Inspection of figure 7 reveals some spatial distortion in the nearfield of the crawling wave sonoelastograms (due to boundary conditions) but high SNR shear wave interference patterns from a depth of 5 to 30 mm can

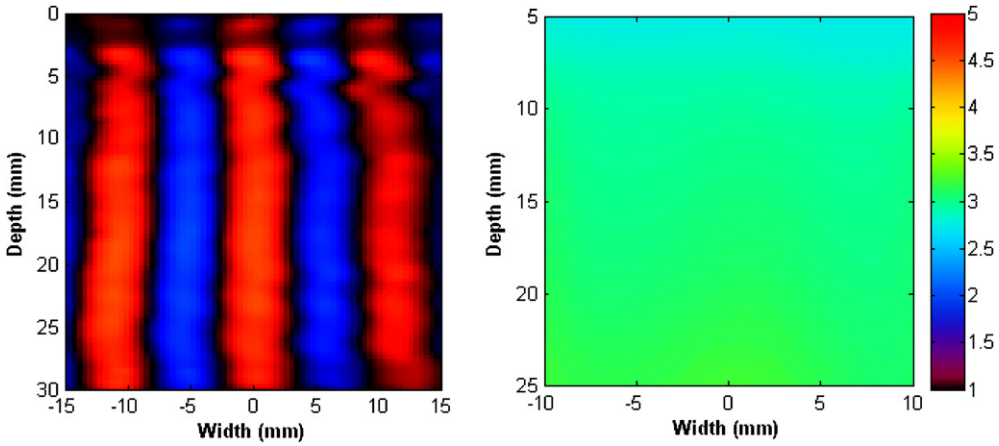

Figure 7. Experimental (a) crawling wave and (b) shear wave speed sonoelastogram (averaged over one wavelength of crawling wave motion) for a source vibration frequency of 140 Hz.

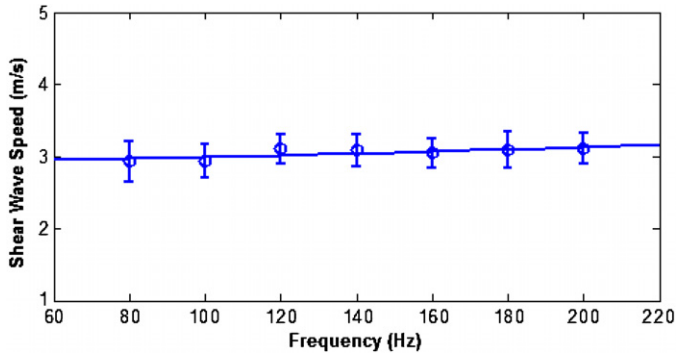

Figure 8. Summary of sonoelastographic shear wave speed estimates in tissue-mimicking phantom that were measured at vibration frequencies of 80 to 200 Hz. The curve represents a best-fit line for the Voigt model, which accounts for both elastic and viscous behavior.

be approximated as plane waves. Within this field-of-view, the averaged shear wave speed sonoelastograms (over one wavelength of crawling wave motion) exhibit a uniform distribution (3.08 ± 0.22 m s^{-1}). Congruence between simulated and experimental results for matched conditions and system parameters, figures 5 and 7, respectively, supports the simulation program developed for this novel shear wave excitation strategy.

A summary of the shear wave speed estimates plotted as a function of frequency and the viscoelastic model fit are shown in figure 8. These results illustrate a slight trend of increasing shear wave speed estimates as a function of vibration frequency, which is suggestive of a viscoelastic response. Note that given the error bars associated with this data set this increase may not be statistically significant and due to artifact. Using the viscoelastic model, shear modulus and shear viscosity estimates for this phantom material were found to be 8.61 kPa and 2.98 Pa s, respectively. Mechanical testing determined a shear modulus for this phantom material to be 8.7 kPa, which is in agreement (1% error) with the viscoelastic model-based shear modulus estimate obtained using quantitative sonoelastographic techniques. It is important

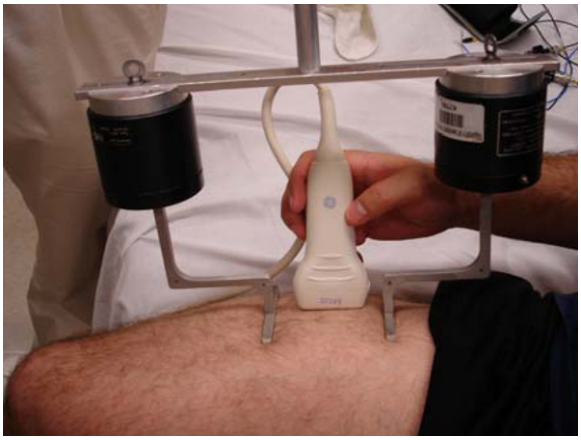

Figure 9. Representative image of the handheld mechanical source pair equipped with surface contacts and ultrasound transducer placement as used for all *in vivo* skeletal muscle experiments.

to note that the mechanical testing method used (based on a compressive force-displacement analysis) does not allow for validation of the viscosity parameter due to the assumption that the material under investigation is linear elastic.

4.2. In vivo skeletal muscle studies

Data were obtained in both relaxed and voluntarily (maximal) contracted skeletal muscles from two healthy adult male volunteers (i.e., without orthopedic or neuromuscular abnormalities) to assess the viscoelastic properties of different muscle tissues and demonstrate clinical utility. Specifically, sonoelastographic data were collected from one volunteer in the following relaxed muscles: rectus femoris, biceps femoris, medial gastrocnemius and biceps brachii. Additionally, data were collected from two healthy adult male volunteers in the following relaxed and then voluntarily (isotonically) contracted muscles: rectus femoris and biceps brachii. For all *in vivo* scans, the mechanical (vibration) source setup was oriented under ultrasound guidance to produce shear wave propagation parallel to the muscle fibers to minimize anisotropic effects (Kruse *et al* 2000, Gennisson *et al* 2003, Hoyt *et al* 2007b). Considering the *in vivo* biceps brachii data presented by Gennisson *et al* (2003), it can be inferred that shear wave speed estimates can decrease by more than 20% when the angle between shear wave propagation and muscle fiber orientation deviates by 10° (i.e., from the parallel shear wave propagation and fiber orientation). Since ultrasonic scattering from skeletal muscle is primarily affected by the endomysial collagen fibers (Hete and Shung 1993, Wang and Shung 1998), it was assumed that by maximizing backscatter continuity (i.e., hyperechogenicity) across the ultrasound image plane that fiber orientation was maintained and registration between relaxed and contracted muscle for a given ROI was established. However, this assumption needs to be investigated further and a more robust technique for ascertaining fiber orientation may be warranted. In order to avoid stress effects to the various muscles investigated, both the mechanical setup and ultrasound scanning were done freehand with care taken to ensure all data were collected under similar boundary conditions and from the same tissue plane (to the extent possible) for each muscle studied. A visual description of the mechanical source pair equipped with surface contacts and transducer placement for *in vivo* skeletal muscle experimentation is depicted in figure 9. Regarding boundary conditions, initial experiences revealed that tissue surface stresses imposed by either the mechanical contacts

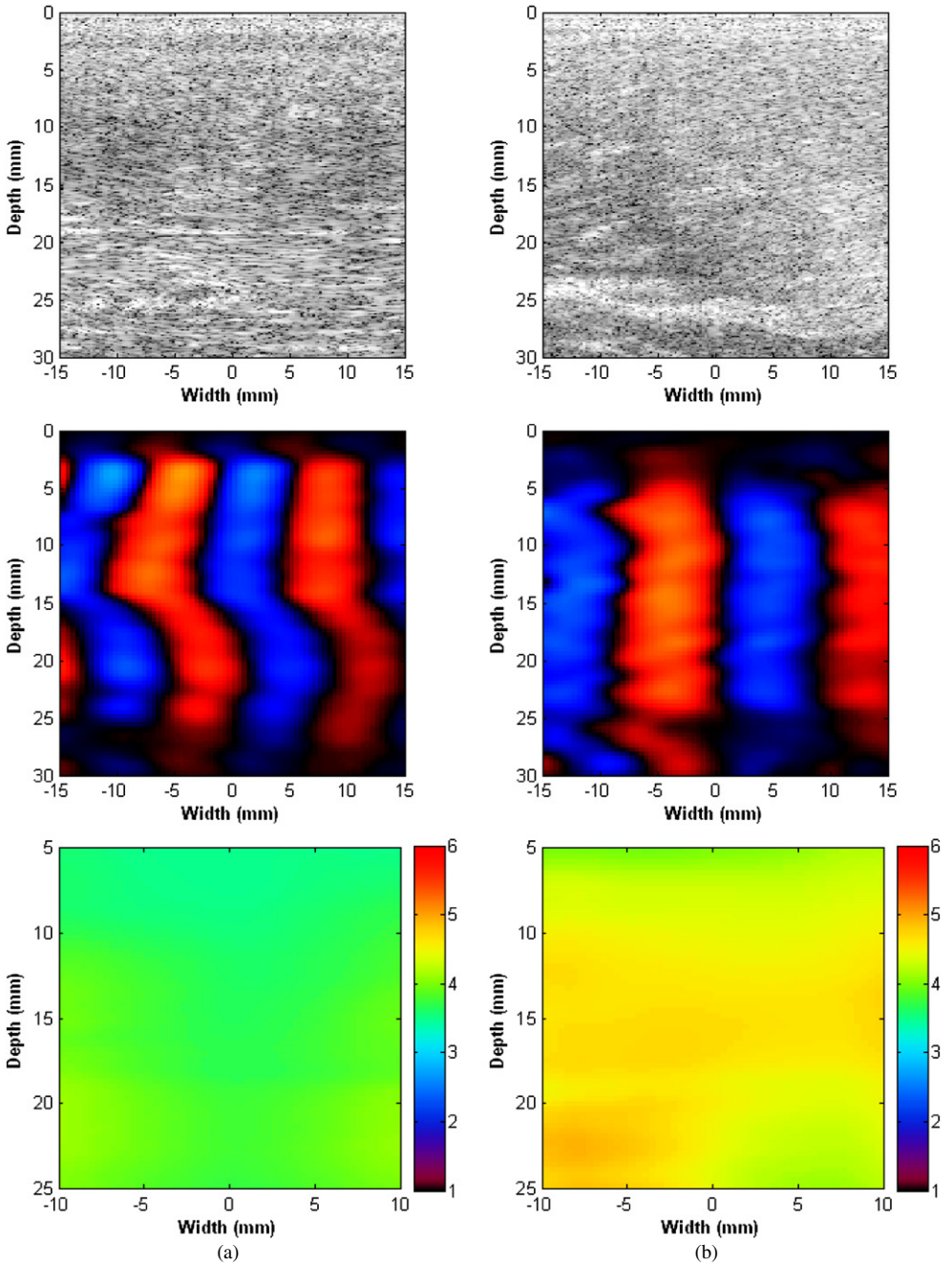

Figure 10. Experimental *in vivo* results (vibration frequency of 140 Hz) obtained from human biceps brachii muscle and depicted for data collected during (a) relaxed and (b) voluntarily contracted states. The subfigures correspond to the matched ultrasound images (top), crawling wave sonoelastograms (middle) and averaged shear wave speed sonoelastograms (units of m s^{-1}) (bottom).

or ultrasound transducer can influence sonoelastographic results by damping the vibrational response (i.e., displacement amplitude) of underlying tissues. For these preliminary *in vivo*

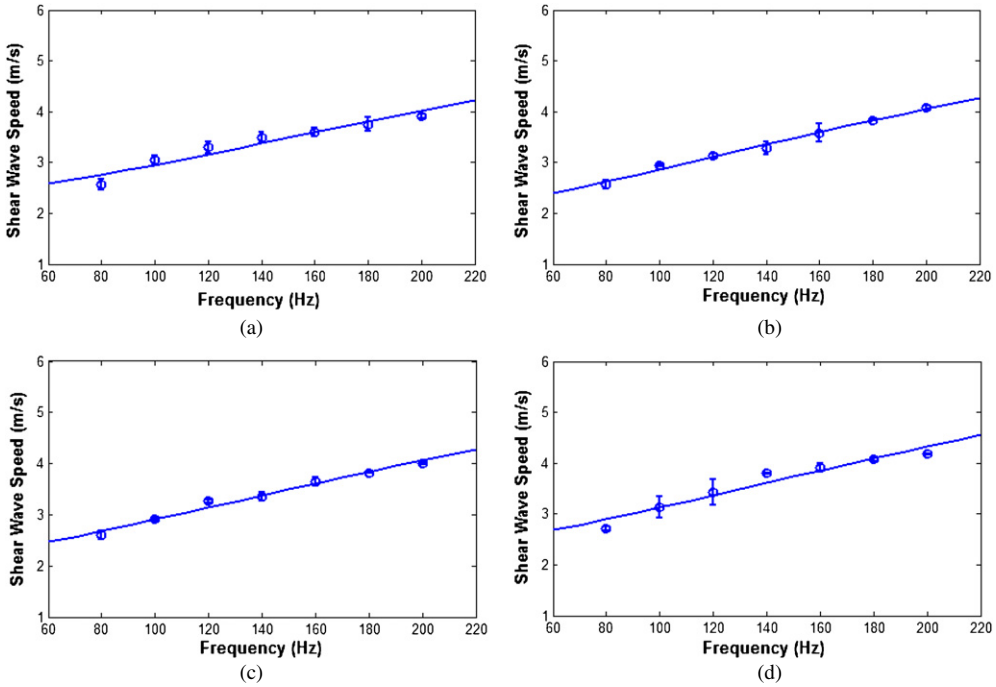

Figure 11. Summary of *in vivo* shear wave speed estimates from healthy human muscle studies. Results are depicted for the following relaxed muscles: (a) rectus femoris, (b) biceps femoris, (c) medial gastrocnemius and (d) biceps brachii. For each plot, the curve represents a best-fit line accounting for muscle viscoelastic behavior.

human studies, data were collected in contralateral muscles and mean shear wave speed estimates (calculated throughout the entire scan sequence and for a chosen image region corresponding to the muscle area of interest) were averaged at each vibration frequency. It is assumed that by averaging contralateral muscle data, shear wave speed variability is minimized, albeit not directly assessed in this study.

A representative set of experimental *in vivo* results obtained from human bicep brachii muscles are shown in figure 10. These results confirm that high-quality sonoelastographic data can be acquired *in vivo* from human muscle tissue. If we consider the dispersive sonoelastographic data collected in relaxed human skeletal muscle tissues and depicted in figure 11, results exhibit minimal variance between data acquisitions from contralateral muscles demonstrating reproducibility despite the freehand-based technique adopted for these studies. Furthermore, the results of figure 11 also reveal a pronounced viscoelastic trend. A summary of the frequency-independent shear modulus and shear viscosity estimates are presented in table 2, which indicates differences between viscoelastic parameters for various (healthy) relaxed skeletal muscles. For comparative purposes, the select shear wave speed estimates of figure 11 are congruent with elasticity imaging-based measurements reported in (or derived from) the literature for both the gastrocnemius (Basford *et al* 2002, Heers *et al* 2003) and biceps brachii (Dresner *et al* 2001, Sack *et al* 2002) muscles (for a given vibration frequency).

Revisiting figure 10, the results presented illustrate that shear wave speeds (at a vibration frequency of 140 Hz) in the relaxed biceps brachii are markedly lower than that for the same

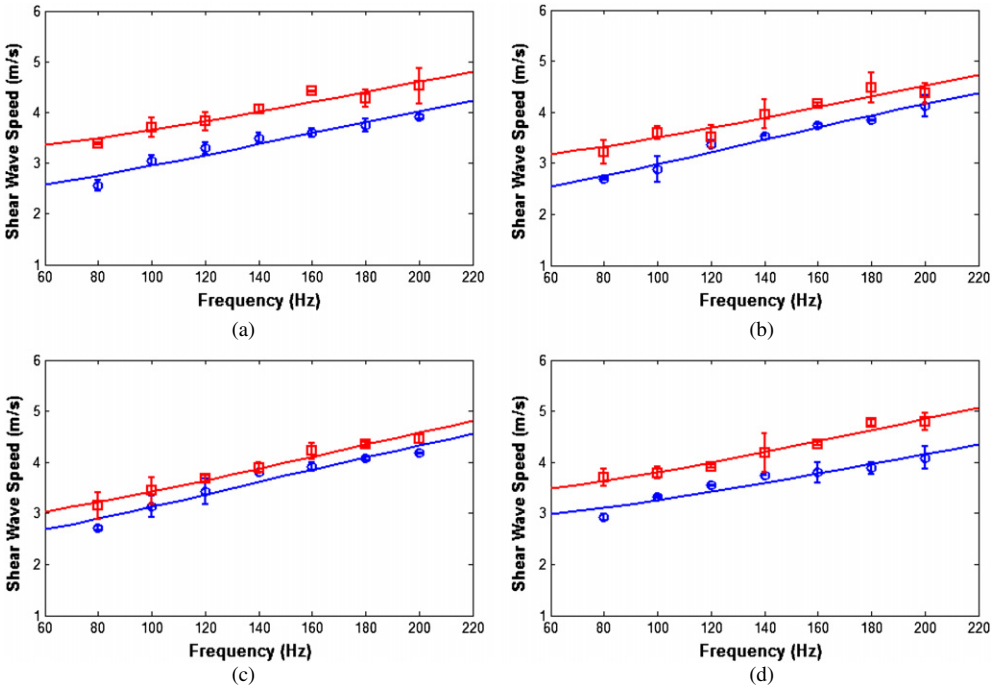

Figure 12. Summary of *in vivo* shear wave speed estimates from human muscle studies. Results from two healthy subjects (top and bottom, respectively) are depicted for the (a) rectus femoris and (b) biceps brachii muscles during states of relaxation (blue) and voluntarily contraction (red). For each plot, the curve represents a best-fit line applied to the relaxed (○) and contracted (□) muscle data that account for any viscoelastic behavior.

Table 2. Shear modulus (μ_1) and shear viscosity (μ_2) estimates obtained from a healthy adult male in various relaxed skeletal muscle tissues.

Muscle name	μ_1 (kPa)	μ_2 (Pa s)
Rectus femoris	5.87	9.14
Biceps femoris	4.45	9.13
Medial gastrocnemius	4.98	9.26
Biceps brachii	6.09	10.55

muscle during a contracted state (3.74 ± 0.31 and 4.45 ± 0.51 m s^{-1}, respectively). Using the viscoelastic model described by equation (12), shear modulus and shear viscosity estimates for the relaxed and contracted biceps brachii muscle data were 8.68 kPa and 9.73 Pa s versus 11.88 kPa and 13.22 Pa s, respectively. Figure 12 illustrates the sonoelastographic data collected from two healthy volunteers in the rectus femoris and biceps brachii muscles during states of relaxation and voluntary (maximal) contraction. Corresponding viscoelastic parameters for the model fits plotted in figure 12 are summarized in table 3. Differences in shear modulus values may be attributed to muscle size (Dresner *et al* 2001) and/or the subjective contractile force (Levinson *et al* 1995, Dresner *et al* 2001, Basford *et al* 2002). Overall, these initial results from healthy volunteers reveal that contracted muscles exhibit

Table 3. Shear modulus (μ_1) and shear viscosity (μ_2) estimates obtained from two healthy adult males (denoted S_1 and S_2) in relaxed and voluntarily contracted skeletal muscle tissue.

	Relaxed		Contracted		Relative change	
Muscle name	μ_1 (kPa)	μ_2 (Pa s)	μ_1 (kPa)	μ_2 (Pa s)	μ_1 (%)	μ_2 (%)
Rectus femoris (S_1)	5.87	9.14	11.17	11.88	90.3	30.0
Biceps brachii (S_1)	6.09	10.55	8.42	11.90	38.3	12.8
Rectus femoris (S_2)	5.33	9.72	9.70	11.60	82.0	19.3
Biceps brachii (S_2)	8.68	9.73	11.88	13.22	36.9	35.9

considerable increases in both shear modulus and shear viscosity estimates as compared to the relaxed state.

5. Conclusions

A novel quantitative sonoelastography technique was introduced. Based on a two mechanical source configuration, theoretical models predicted shear wave interference displacement fields, which were validated through phantom studies. Using dispersive shear wave speed sonoelastographic data, a viscoelastic model (the classical Voigt model) was fit using nonlinear least-squares techniques to determine the frequency-independent shear modulus and shear viscosity estimates. Consequently, shear modulus estimates derived using the Voigt model were in agreement with that obtained by mechanical testing on phantom samples (1.0% error).

Preliminary sonoelastographic data were acquired in healthy human skeletal muscles and results confirm that high-quality quantitative elasticity data can be acquired *in vivo*. Studies on relaxed muscle indicates that discernible differences in both shear modulus and shear viscosity estimates do exist between different relaxed skeletal muscle groups. More importantly, viscoelastic properties for these various muscle groups can be assessed using sonoelastographic techniques. Investigations into the dynamic viscoelastic properties of healthy human skeletal muscles revealed that voluntarily contracted muscles exhibit considerable increases in both shear modulus and shear viscosity estimates as compared to the relaxed state. Overall, preliminary results are encouraging and quantitative sonoelastography may prove clinically feasible for the *in vivo* characterization of the dynamic viscoelastic properties of human skeletal muscle in health and disease.

Acknowledgments

The authors would like to thank Drs Deborah J Rubens and John Strang for their insightful comments. This work was supported in part by NIH Grant 5 R01 AG16317–07.

References

Basford J R, Jenkyn T R, An K, Ehman R L, Heers G and Kaufman K R 2002 Evaluation of healthy and diseased muscle with magnetic resonance elastography *Arch. Phys. Med. Rehabil.* **83** 1530–6

Bensamoun S F, Ringleb S I, Chen Q, Ehman R L, An K and Brennan M 2007 Thigh muscle stiffness assessed with magnetic resonance elastography in hyperthyroid patients before and after medical treatment *J. Magn. Reson. Imaging* **26** 708–13

Bensamoun S F, Ringleb S I, Littrell L, Chen Q, Brennan M, Ehman R L and An K 2006 Determination of thigh muscle stiffness using magnetic resonance elastography *J. Magn. Reson. Imaging* **23** 242–7

Catheline S, Gennisson J L, Delon G, Fink M, Sinkus R, Abouelkaram S and Culioli J 2004 Measurement of viscoelastic properties of homogeneous soft solid using transient elastography: an inverse problem approach *J. Acoust. Soc. Am.* **116** 3734–41

Dresner M A, Rose G H, Rossman P J, Muthupillai R, Manduca A and Ehman R L 2001 Magnetic resonance elastography of skeletal muscle *J. Magn. Reson. Imaging* **13** 269–76

Fung Y C 1993 *Biomechanics: Mechanical Properties of Living Tissue* (New York: Springer)

Gao L, Parker K J, Lerner R M and Levinson S F 1996 Imaging of the elastic properties of tissue: A review *Ultrasound Med. Biol.* **22** 959–77

Gennisson J L, Catheline S, Chaffai S and Fink M 2003 Transient elastography in anisotropic medium: application to the measurement of slow and fast shear wave speeds in muscles *J. Acoust. Soc. Am.* **114** 536–41

Gennisson J L, Lerouge S and Cloutier G 2006 Assessment by transient elastography of the viscoelastic properties of blood during clotting *Ultrasound Med. Biol.* **32** 1529–37

Greenleaf J F and Chen S 2007 Measurement of mechanical properties of homogeneous tissue with ultrasonically induced shear waves *Proc. SPIE* **6513** 65130F-1

Greenleaf J F, Fatemi M and Insana M 2003 Selected methods for imaging elastic properties of biological tissues *Annu. Rev. Biomed. Eng.* **5** 57–78

Heers G, Jenkyn T, Dresner M A, Klein M, Basford J R, Kaufman K R, Ehman R L and An K 2003 Measurement of muscle activity with magnetic resonance elastography *Clin. Biomech.* **18** 537–42

Hete B and Shung K K 1993 Scattering of ultrasound from skeletal muscle tissue *IEEE Trans. Ultrason. Ferroelectr. Freq. Control* **40** 354–65

Hoyt K, Castaneda B and Parker K J 2008 Two-dimensional sonoelastographic shear velocity imaging *Ultrasound Med. Biol.* **34** 276–88

Hoyt K, Parker K J and Rubens D J 2007a Real-time shear velocity imaging using sonoelastographic techniques *Ultrasound Med. Biol.* **33** 1086–97

Hoyt K, Castaneda B and Parker K J 2007b Muscle tissue characterization using quantitative sonoelastography: preliminary results *IEEE Ultrason. Symp.* vol 1 pp 365–8

Hoyt K and Parker K J 2007 Lesion contrast and detection using sonoelastographic shear velocity imaging: preliminary results *Proc. SPIE* **6513** 65130L-1

Huang S R, Lerner R M and Parker K J 1990 On estimating the amplitude of harmonic vibration from the Doppler spectrum of reflected signals *J. Acoust. Soc. Am.* **88** 310–7

Jenkyn T R, Ehman R L and An K 2003 Noninvasive muscle tension measurement using the novel technique of magnetic resonance elastography (MRE) *J. Biomechanics* **36** 1917–21

Kasai C, Namekawa K, Koyano A and Omoto R 1985 Real-time two-dimensional blood flow imaging using an autocorrelation technique *IEEE Trans. Sonics Ultrason.* **32** 458–64

Krouskop T A, Wheeler T M, Kallel F, Garra B S and Hall T 1998 Elastic moduli of breast and prostate tissues under compression *Ultrason. Imaging* **20** 260–74

Kruse S A, Smith J A, Lawrence A J, Dresner M A, Manduca A, Greenleaf J F and Ehman R L 2000 Tissue characterization using magnetic resonance elastography: preliminary results *Phys. Med. Biol.* **45** 1579–90

Lakes R S 1998 *Viscoelastic Solids* (Boca Raton, FL: CRC Press LLC)

Lerner R M, Parker K J, Holen J, Gramiak R and Waag R C 1988 Sonoelasticity: medical elasticity images derived from ultrasound signals in mechanically vibrated targets *Acoust. Imaging* **16** 317–27

Levinson S F, Shinagawa M and Sato T 1995 Sonoelastic determination of human skeletal muscle elasticity *J. Biomech.* **28** 1145–4

Madsen E L, Sathoff H J and Zagzebski J A 1983 Ultrasonic shear wave properties of soft tissues and tissuelike materials *J. Acoust. Soc. Am.* **74** 1346–55

Marple S L 1999 Computing the discrete-time analytic signal via FFT *IEEE Trans. Signal Process.* **47** 2600–3

Miller G F and Pursey H 1954 The field and radiation impedance of mechanical radiators on the free surface of a semi-infinite isotropic solid *Proc. R. Soc. Lond.* A **233** 521–41

Oestreicher H L 1951 Field and impedance of an oscillating sphere in a viscoelastic medium with an application to biophysics *J. Acoust. Soc. Am.* **23** 707–14

Ophir J, Alam S K, Garra B, Kallel F, Konofagou E, Krouskop T and Varghese T 1999 Elastography: Ultrasonic estimation and imaging of the elastic properties of tissues *Proc. Inst. Mech. Eng.* **213** 203–33

Parker K J, Fu D, Gracewski S M, Yeung F and Levinson S F 1998 Vibration sonoelastography and the detectability of lesions *Ultrasound Med. Biol.* **24** 1937–47

Phipps S, Yang T H J, Habib F K, Reuben R L and McNeill S A 2005 Measurement of tissue mechanical characteristics to distinguish between benign and malignant prostatic disease *J. Urol.* **66** 447–50

Sack I, Bernarding J and Braun J 2002 Analysis of wave patterns in MR elastography of skeletal muscle using couple harmonic oscillator simulations *J. Magn. Reson. Imaging* **20** 95–104

Sarvazyan A P, Rudenko O V, Swanson S D, Fowlkes J B and Emelianov S Y 1998 Shear wave elasticity imaging: a new ultrasonic technology of medical diagnostics *Ultrasound Med. Biol.* **24** 1419–35

Taylor L S, Porter B C, Rubens D J and Parker K J 2000 Three-dimensional sonoelastography: Principles and practices *Phys. Med. Biol.* **45** 1477–94

Wang C Y and Shung K K 1998 Variation in ultrasonic backscattering from skeletal muscle during passive stretching *IEEE Trans. Ultrason. Ferroelectr. Freq. Control* **45** 504–10

Wu Z, Hoyt K, Rubens D J and Parker K J 2006 Sonoelastographic imaging of interference patterns for estimation of shear velocity distribution in biomaterials *J. Acoust. Soc. Am.* **120** 535–45

Wu Z, Taylor L S, Rubens D J and Parker K J 2004 Sonoelastographic imaging of interference patterns for estimation of the shear velocity of homogeneous biomaterials *Phys. Med. Biol.* **49** 911–22

Zhang M, Nigwekar P, Castaneda B, Hoyt K, Sant'Agnese A, Joseph J V, Messing E M, Rubens D J and Parker K J 2008 Quantitative characterization of viscoelastic properties of human prostate correlated with histology *Ultrasound Med. Biol.* in press doi:10.1016/j.ultrasmedbio.2007.11.024